

A HIGH ORDER NUMERICAL SCHEME FOR INCOMPRESSIBLE NAVIER-STOKES EQUATIONS

H. Khurshid^{1*}, K. A. Hoffmann²

^{1,2}Department of Aerospace Engineering,
Wichita State University, Wichita, Kansas,
67260-0044, USA

ABSTRACT

To solve the incompressible Navier-Stokes equations in a generalized coordinate system, a high order solver is presented. An exact projection method/fractional-step scheme is used in this study. Convective terms of the Navier-Stokes (N-S) equations are solved using fifth-order WENO spatial operators, and for the diffusion terms, a sixth-order compact central difference scheme is employed. The third-order Runge-Kutta (R-K) explicit time-integrating scheme with total variation diminishing (TVD) is adopted for the unsteady flow computations. The advantage of using a WENO scheme is that it can resolve applications using less number of grid points. Benchmark cases such as, driven cavity flow, Taylor-Green (TG) vortex, double shear layer, backward-facing step, and skewed cavity are used to investigate the accuracy of the scheme for two dimensional flow.

KEYWORDS: *WENO; Incompressible flow; Generalized coordinates; Finite difference; Shear layer problem*

1.0 INTRODUCTION

The restriction to the incompressible flow introduces the computational difficulty that the continuity equation contains only velocity components and there is no obvious link with the pressure as there is for compressible equations. To overcome this restriction various numerical schemes are available to obtain the numerical solution of incompressible Navier-Stokes (N-S) equations. These include the marker and cell (MAC) method, spectral methods, semi-implicit method for pressure linked equations (SIMPLE), methods that use stream functions and vorticity variables, and exact projection methods. The exact projection method was originally proposed by Chorin (1968) for incompressible, unsteady (N-S) equations, and subsequently it was further investigated by Drikakis and Rider (2005). This method is stable

* Corresponding author email: hassankim@yahoo.com

and can be used in applications with difficult boundary conditions. Therefore, in the current effort, a form of projection method, referred to as the fractional-step scheme, by Moin and Kim (1984), is adopted with the collocated grid.

Traditional linearly stable schemes, such as spectral methods (Harlow and Welsh 1965; Orszag and Israeli, 1974) and high-order spatial central difference methods (Moin and Kim 1980; Rogers, 1990) are suitable for cases where the solution can be fully resolved, but typically produces signs of instability when small-scale features of the flow, such as shears and roll-ups, cannot be adequately resolved on the computational grid. Although, in principle, one can always overcome this difficulty by refining the grid, today's computer capacity seriously restricts the largest possible domain size. For high Reynolds number flows or flows with strong shear, these schemes do not provide accurate results. As is well known, the high resolution shock capturing schemes, such as essentially non-oscillatory (ENO) and weighted essentially non-oscillatory (WENO) schemes, are based on the philosophy of giving up fully resolving rapid transition regions or shocks, just to capture them in a stable and somehow globally correct fashion, but, at the same time, requiring a high resolution for the smooth part of the solution. The success of such an approach for conservation laws is documented by several researchers (Shu and Osher, 1989; Shu et al., 1992). The conclusion seems to be that, when fully resolving a flow that is either impossible or too costly, a capturing scheme such as ENO can be used on a coarse grid to obtain at least some partial information about it. Thus, it is expected that, for the incompressible flow, one can use high-order ENO or WENO schemes on a coarse grid, without fully resolving the flow, but obtaining useful information.

Pioneering work in applying shock capturing compressible flow techniques to incompressible flows was performed by Bell et al. (1989), who considered a second-order Godunov type discretization, investigated the projection into divergence-free velocity fields for general boundary conditions, and discussed the accuracy of time discretizations. Higher-order ENO and WENO schemes for incompressible flows are extensions of such methods.

ENO schemes were introduced by Harten et al. (1987) in the form of cell averages. Their procedure used an adaptive stencil of grid points, and consequently, the resulting schemes were highly non-linear. Since the publication of that original paper, the authors and many other researchers have followed this pioneering work, improving the methodology and expanding the range of its applications. ENO

schemes are high order accurate; however, they have some drawbacks, as outlined by Jiang and Shu (1996). The stencil may change, even by a round-off error perturbation near zeroes of the solution and its derivatives. This may cause loss of accuracy when applied to a hyperbolic partial differential equation (PDE). The ENO scheme was modified to the WENO scheme by Jiang and Shu (1996). In the WENO scheme, instead of using only one candidate stencil, a convex combination of all candidate stencils is used. Each of the candidate stencils is assigned a weight, which determines the contribution of this stencil to the final approximation of the numerical flux. Weights are defined in such a way that, in smooth regions, they approach certain optimal weights to achieve a high order of accuracy, while in the region near discontinuities, stencils that contain the discontinuities are assigned a nearly zero weight. The WENO scheme has been further improved by Arshed and Hoffmann (2009) who improved the accuracy of the WENO scheme near the critical points and also reduced the severe smearing at contact discontinuities.

The WENO scheme is a shock capturing scheme, however, more recently it has been used in solving incompressible flows as well. Chen et al. (1999) used implicit WENO schemes to solve incompressible Navier-Stokes equations by selecting their algorithm on the artificial compressibility formulation. They presented a class of lower-upper/approximate factorization implicit WENO scheme. Symmetric Gauss-Seidel relaxation was used to compute steady state solutions, while symmetric successive over relaxation was used to treat time dependent flows. Hsieh et al. (2008) investigated several variants of WENO schemes numerically for Euler equations.

In the current effort, the WENO scheme of Shu (1997) is adopted and applied to solve incompressible flow problems. Flux splitting is used, and the WENO scheme is applied to the convective terms without introducing artificial compressibility. This is the main difference in the method as compared to Chen et al. (1999) that makes the implementation simpler. In addition, the resulting scheme has been tested not only on the simple rectangular geometries but also on complex geometries such as skewed cavity where coordinate transformation is required. It has been shown that by using WENO scheme the results are obtained with lesser number of grids as compared to the grids used in the existing literature. A sixth-order compact scheme is applied to solve the viscous terms. The fractional-step scheme in conjunction with third-order Runge Kutta (R-K) total variation diminishing (TVD) is used for the time discretization. The R-K TVD is generally good, since it preserves the variation. The present effort does not include supersonic

effects; therefore, the sound speed is infinite, and hence, the artificial compressibility factor is not required. The resulting scheme is applied to standard incompressible flow problems.

2.0 NUMERICAL PROCEDURE

The conservation of momentum and conservation of mass equations can be used to describe any incompressible flow. The N-S equations are mathematically expressed as:

$$\frac{\partial u_i}{\partial t} + \frac{\partial(u_i u_j)}{\partial x_j} = -\frac{\partial p}{\partial x_i} + \frac{1}{Re} \frac{\partial^2 u_i}{\partial x_j \partial x_j} \quad (1)$$

$$\frac{\partial u_i}{\partial x_i} = 0 \quad (2)$$

where u_i is the non-dimensional velocity with ($i = 1, 2$) representing two coordinate directions, and p is the non-dimensional pressure. The relation $Re = UL/\nu$ is the Reynolds number based on some characteristic velocity U , characteristic length L , and kinematics viscosity ν . In essence, to resolve the incompressible flow, it is necessary to solve equation (1) and (2) for velocity and pressure with appropriate boundary and initial conditions. However, in practice, the given equations are a set of coupled non-linear time dependent PDEs for which there are no known analytical solutions, and one must resort to numerical techniques to solve them.

In the case of two-dimensional incompressible flows, one needs to solve the Navier-Stokes equation for two coordinate velocities, say u, v , and the pressure field p . Equation (1), which represents the momentum along the two coordinate directions, can be used to solve for two components of velocity; however, there is no explicit equation for pressure. Mathematically speaking, if a correct pressure field is known, equation (1) will provide a velocity field, which will be divergence free, or in other words, it will satisfy equation (2).

Several algorithms are available that result in pressure and velocity fields satisfying equation (1) and (2). The exact projection method is one such algorithm originally proposed by Chorin (1968) for incompressible, unsteady Navier-Stokes equations. In order to satisfy the incompressibility condition, the fractional-step process described in the paper of Kim and Moin (1984) is incorporated at each stage of Runge Kutta. According to this approach, the goal is to advance the

velocity vector field $V = V(u,v)$ by a reasonable mean, disregarding the non-solenoidal nature of V (meaning that V will not satisfy equation (2)). For this purpose, equation (1) can be used by simply dropping the term $\frac{\partial p}{\partial x_i}$ and using the previous time step velocities to calculate the velocities for the next time step.

The pressure projection method allows splitting the N-S equation into two sets of equations where pressure and velocity are separated. This can be achieved by integrating equation (1) in time interval Δt as

$$(u_i)^{n+1} = (u_i)^n + \int_t^{t+\Delta t} \left(-\frac{\partial u_i u_j}{\partial x_j} + \frac{1}{\text{Re}} \frac{\partial^2 u_i}{\partial x_j \partial x_j} \right) dt - \frac{\partial p}{\partial x_i} \Delta t \quad (3)$$

where $(u_i)^n$ is the velocity at time t or at numerical step n , which is known, and $(u_i)^{n+1}$ is unknown and is the velocity at the next time step $n+1$ or, generally, at time $t+\Delta t$. Furthermore, the right side shows an integral that can be found by means of any numerical integration (here the Runge-Kutta will be employed) and space derivative of mean pressure P in the interval Δt . The two first terms on the right side can be denoted by u_i^*

$$(u_i)^* = (u_i)^n + \int_t^{t+\Delta t} \left(-\frac{\partial u_i u_j}{\partial x_j} + \frac{1}{\text{Re}} \frac{\partial^2 u_i}{\partial x_j \partial x_j} \right) dt \quad (4)$$

and equation (3) is reduced to

$$(u_i)^{n+1} = (u_i)^* - \frac{\partial P}{\partial x_i} \Delta t \quad (5)$$

and is also called velocity correction. Now taking the divergence of equation 5 as

$$\frac{\partial (u_i)^{n+1}}{\partial x_i} = \frac{\partial (u_i)^*}{\partial x_i} - \frac{\partial^2 P}{\partial x_i \partial x_i} \Delta t \quad (6)$$

Since it is known, from the continuity equation, that the divergence of velocity at any time step (specifically here at $n+1$) is zero, the left side is zero and a relation between mean pressure P and intermediate velocity u_i^* is established as

$$\frac{\partial^2 P}{\partial x_i \partial x_i} = \frac{1}{\Delta t} \frac{\partial (u_i)^*}{\partial x_j} \tag{7}$$

Equation (4) for $(u_i)^*$ is expressed in a differential form instead of the integral form as,

$$\frac{\partial u_i}{\partial t} \Big|_* = \frac{\partial u_i u_j}{\partial x_j} + \frac{1}{\text{Re}} \frac{\partial^2 u_i}{\partial x_j \partial x_j} \tag{8}$$

Thus, the governing equations to be solved numerically for an incompressible flow composed of equation (5)-(8) are

$$\frac{\partial u_i}{\partial t} \Big|_* = \frac{\partial u_i u_j}{\partial x_j} + \frac{1}{\text{Re}} \frac{\partial^2 u_i}{\partial x_j \partial x_j} \tag{9}$$

$$\frac{\partial^2 P}{\partial x_i \partial x_i} = \frac{1}{\Delta t} \frac{\partial (u_i)^*}{\partial x_j} \tag{10}$$

$$(u_i)^{n+1} = (u_i)^* - \frac{\partial P}{\partial x_i} \Delta t \tag{11}$$

To solve the above system of equations, Runge-Kutta integration is used for the first equation in order to obtain $(u_i)^*$. Subsequently, the second equation is solved by the Poisson solver to obtain pressure P . Finally the last equation is used to calculate velocity at the next time step $(u_i)^{n+1}$. This is a brief approach to the solution. A more detailed description in a two-dimensional general coordinate system is provided next. To express equations in a two-dimensional general coordinate system and in a useful form for WENO schemes, the equation of fluid motion excluding the pressure term can be expressed in a flux vector form as

$$\frac{\partial Q}{\partial t} = \frac{\partial (E_v - E)}{\partial x} + \frac{\partial (F_v - F)}{\partial y} \tag{12}$$

$$Q = \begin{bmatrix} u \\ v \end{bmatrix} \quad E = \begin{bmatrix} u^2 \\ uv \end{bmatrix} \quad F = \begin{bmatrix} uv \\ v^2 \end{bmatrix} \tag{13}$$

where

$$E_v = \text{Re}^{-1} \begin{bmatrix} 2u_x \\ u_y + v_x \end{bmatrix} \quad F_v = \text{Re}^{-1} \begin{bmatrix} v_x + u_y \\ 2v_y \end{bmatrix}$$

where u, v are velocities in the Cartesian coordinate system, and indexes (x, y) denote derivatives with respect to that index, e.g., $v_x = dv/dx$. Conventionally, equation (12) is transformed into the generalized coordinates (ξ, η) as

$$\frac{\partial \hat{Q}}{\partial t} = \frac{\partial(\hat{E}_v - \hat{E})}{\partial \xi} + \frac{\partial(\hat{F}_v - \hat{F})}{\partial \eta} \tag{14}$$

where

$$\begin{aligned} \hat{Q} &= J \begin{bmatrix} u \\ v \end{bmatrix} & \hat{E} &= J \begin{bmatrix} uU \\ vU \end{bmatrix} & \hat{F} &= J \begin{bmatrix} uV \\ vV \end{bmatrix} \\ \hat{E}_v &= J [\xi_x E_v + \xi_y F_v] & \hat{F}_v &= J [\eta_x E_v + \eta_y F_v] \\ U &= \xi_x u + \xi_y v, & V &= \eta_x u + \eta_y v, & J &= |x_\xi x_\eta, y_\xi y_\eta| \end{aligned} \tag{15}$$

The derivative operator is used in equation (7) to solve the Poisson equation. Therefore, the operator of the second derivative γ acting on pressure P is on the left side, and the right hand term is constructed according to coordinate system transformation as

$$\gamma P = \frac{1}{J \Delta t} \left(\frac{\partial(JU)}{\partial \xi} + \frac{\partial(JV)}{\partial \eta} \right) \tag{16}$$

The derivative operator is

$$\gamma = \frac{\partial}{\partial q_j} \left(\frac{\partial}{\partial q_k} \frac{\partial q_k}{\partial x_i} \right) \frac{\partial q_j}{\partial x_i} \tag{17}$$

where $i, j, k = \{1, 2\}$, $q_1 = \xi$ and $q_2 = \eta$

The operator is also a double first derivative operator; hence, the following relation is true:

$$\gamma = d^{xi} d^{xi} \tag{18}$$

$$d^{xi} = \frac{\partial}{\partial q_j} \frac{\partial q_j}{\partial x_i} \tag{19}$$

Equation (18) and (19) are used in the Poisson solver, and subsequently, equation (5) simply becomes

$$\begin{aligned} (u)^{n+1} &= (u)^* - (P_\xi \xi_x + P_\eta \eta_x) \Delta t \\ (v)^{n+1} &= (v)^* - (P_\xi \xi_y + P_\eta \eta_y) \Delta t \end{aligned} \tag{20}$$

The spatial discretization of the convective term is performed by using a fifth order WENO scheme with local Lax-Friedrichs. Fluxes are computed in the characteristic fields and at the interface point. The field's Jacobian must be estimated by Roe average. The objective in the convective portion of the equation is to find derivatives of the fluxes: $\frac{\partial \hat{E}}{\partial \xi}$ and $\frac{\partial \hat{F}}{\partial \eta}$. Generally, the derivative of a flux (say \hat{E}) can be found by numerical approximation of this form

$$\frac{\partial \hat{E}}{\partial \xi} = \frac{\hat{E}_{i+1/2} - \hat{E}_{i-1/2}}{\Delta \xi} \tag{21}$$

where $\hat{E}_{i+1/2}$ and $\hat{E}_{i-1/2}$ are the interface fluxes, which are calculated using the WENO scheme. Similar treatment is applied to the derivative of \hat{F} . Viscous fluxes \hat{E}_v and \hat{F}_v are determined using the compact scheme. Depending on the direction in which the information is propagating, the interface fluxes in WENO are given as:

$$\begin{aligned} v_{i+1/2}^- &= \omega_0(l) \left(\frac{1}{3} v_i + \frac{5}{6} v_{i+1} - \frac{1}{6} v_{i+2} \right) + \omega_1(l) \left(-\frac{1}{6} v_{i-1} + \frac{5}{6} v_i + \frac{1}{3} v_{i+1} \right) + \\ &\omega_2(l) \left(\frac{1}{3} v_{i-2} - \frac{7}{6} v_{i-1} + \frac{11}{6} v_i \right), \end{aligned} \tag{22}$$

$$\begin{aligned} v_{i-1/2}^+ &= \omega_0(l) \left(\frac{11}{6} v_i - \frac{7}{6} v_{i+1} + \frac{1}{3} v_{i+2} \right) + \omega_1(l) \left(\frac{1}{3} v_{i-1} + \frac{5}{6} v_i - \frac{1}{6} v_{i+1} \right) + \\ &\omega_2(l) \left(-\frac{1}{6} v_{i-2} + \frac{5}{6} v_{i-1} + \frac{1}{3} v_i \right). \end{aligned} \tag{23}$$

where $\omega_r(l)$ are the non-linear weights, which are defined by

$$\omega_r(l) = \frac{\alpha_r(l)}{\sum_{m=0}^{k-1} \alpha_m(l)}, \quad r = 0, \dots, k-1 \tag{24}$$

with

$$\alpha_r(l) = \frac{d_r}{(\varepsilon + \beta_r(l))^2} \tag{25}$$

Here, $\varepsilon = 10^{-40}$; and $d_r \geq 0$ is the optimal weight that satisfies the requirement that $\sum_{r=0}^{k-1} d_r = 1$. The term $\beta_r(l)$ is called the smoothness indicator. For $k = 3$,

$$\begin{aligned} \beta_0(l) &= \frac{13}{12}(v_l - 2v_{l+1} + v_{l+2})^2 + \frac{1}{4}(3v_l - 4v_{l+1} + v_{l+2})^2, \\ \beta_1(l) &= \frac{13}{12}(v_{l-1} - 2v_l + v_{l+1})^2 + \frac{1}{4}(v_{l-1} - v_{l+1})^2, \\ \beta_2(l) &= \frac{13}{12}(v_{l-2} - 2v_{l-1} + v_l)^2 + \frac{1}{4}(v_{l-2} - 4v_{l-1} + 3v_l)^2. \end{aligned} \tag{26}$$

If $k = 3$ and the information is propagating from left to right, then the optimal weights are $d_0 = \frac{3}{10}, d_1 = \frac{3}{5}$, and $d_2 = \frac{1}{10}$, and if the information is propagating from right to left, then they are, $d_0 = \frac{1}{10}, d_1 = \frac{3}{5}$, and $d_2 = \frac{3}{10}$. When using the WENO scheme, the physical fluxes (E and F) are split locally into positive and negative segments as:

$$F(Q) = F^+(Q) + F^-(Q) \tag{27}$$

where $\frac{\partial F^+}{\partial Q} \geq 0$ and $\frac{\partial F^-}{\partial Q} \leq 0$. Several flux splitting methods can be used. In the current efforts, the Lax-Friedrichs flux splitting method is utilized.

$$F^\pm(Q) = \frac{1}{2}(F(Q) + |\Lambda|Q) \tag{28}$$

where $|\Lambda| = \text{diag}(|\lambda_1|, |\lambda_2|, |\lambda_3|)$ and λ_1, λ_2 and λ_3 are local eigenvalues.

Particularly in the code, the matrix of flux is \hat{E}

$$\begin{bmatrix} |\xi_x u + \xi_y v| & 0 \\ 0 & 2|\xi_x u + \xi_y v| \end{bmatrix} \tag{29}$$

The matrix for flux \hat{F} is

$$\begin{bmatrix} |\eta_x u + \eta_y v| & 0 \\ 0 & 2|\eta_x u + \eta_y v| \end{bmatrix} \quad (30)$$

and the maximum is taken over seven neighboring points. Once the fluxes are split, the WENO interpolation can be performed. However, the interpolation must be performed in the local characteristic field. Therefore, right (r) and left (l) eigenvectors of the field in the interpolated points ($i \pm 1/2$) are required. For flux \hat{E} the eigenvectors are

$$r = \begin{bmatrix} -\bar{\xi}_y & \bar{u} \\ \bar{\xi}_x & \bar{v} \end{bmatrix}, \quad l = \frac{1}{\bar{u}\bar{\xi}_x + \bar{v}\bar{\xi}_y} \begin{bmatrix} -\bar{v} & \bar{u} \\ \bar{\xi}_x & \bar{\xi}_y \end{bmatrix} \quad (31)$$

where quantities with bars are at points $i \pm 1/2$, and their values are the means of neighbors, e.g., $\bar{u}_{i+1/2} = \frac{u_i + u_{i+1}}{2}$ in direction ξ . Similarly, for flux \hat{F} ,

$$r = \begin{bmatrix} -\bar{\eta}_y & \bar{u} \\ \bar{\eta}_x & \bar{v} \end{bmatrix}, \quad l = \frac{1}{\bar{u}\bar{\eta}_x + \bar{v}\bar{\eta}_y} \begin{bmatrix} -\bar{v} & \bar{u} \\ \bar{\eta}_x & \bar{\eta}_y \end{bmatrix} \quad (32)$$

where, the mean is taken along the η direction.

The viscous segment of the N-S equation is calculated by means of the sixth order compact scheme. For this purpose, a differential operator is created, which acts on the velocity field in order to find the derivative. To create the required operator, one begins from the definition of compact schemes

$$\alpha f'_{i-1} + f'_i + \alpha f'_{i+1} = b \frac{f_{i+2} - f_{i-2}}{4\Delta x} + a \frac{f_{i+1} - f_{i-1}}{2\Delta x} \quad (33)$$

where f is any function, f' is its derivative, Δx is grid size, i is the grid node index, and values α , a , and b are coefficients depending on the order and type of scheme (for the sixth order scheme, $\alpha = 1/3$, $a = 14/9$ and $b = 1/9$). The only unknown is f' . The equation is written in the matrix form as

$$L f' = R f \quad (34)$$

where L, R are known square matrices and f, f' are vectors. Multiplying both sides by the inverse of L provides

$$f' = L^{-1}Rf = Df \tag{35}$$

Now, $D = L^{-1}R$ is the differential operator. The D operator is created at the beginning of the procedure for both directions $\xi(D^\xi)$ and $\eta(D^\eta)$. To calculate u_x in the general coordinate system, one is performing (according to nested differentiation rules)

$$u_x = (D^\xi u)\xi_x + (D^\eta u)\eta_x \tag{36}$$

The same is true for the remaining variables (u_y, v_x, v_y) , which are required to calculate E_v and F_v defined in equation (13) and are necessary for calculating of \hat{E}_v and \hat{F}_v . The derivative of the flux is simply calculated by the formula

$$\frac{\partial E_v}{\partial \xi} = D^\xi \hat{E}_v \tag{37}$$

The last step to solving equation (14) is to integrate the equation in time. In this effort, the time discretization of the scheme is implemented by the optimal third order TVD Runge Kutta method developed by Shu and Osher (1989).

One must remember that, in this case, the N-S equation, without the pressure term, is not considered alone but is coupled with the Poisson equation and pressure correction. To properly solve such a system of equations, each intermediate step of R-K must be accompanied by solution of the Poisson equation and pressure correction. In order to solve the Poisson equation, one needs to find the intermediate velocity using the RK method. Velocity is used to find the right hand side of equation (16); derivatives are calculated by means of compact schemes. The right hand side forms a matrix S . By finding an inverse of the derivative operator Υ , one can resolve equation (16) with respect to P as

$$P = \Upsilon^{-1}S \tag{38}$$

To calculate the right hand side S of equation (16) the compact scheme and its operator D are used. The operator is applied as described previously, so the right hand side becomes

$$S = \frac{1}{J\Delta t} (D^{\dagger}(JU) + (JV)D^{\dagger}) \quad (39)$$

The derivative operator Υ is constructed, based on compact schemes and defined as the multiplication of two first order operators. Once the Υ operator is constructed, the Poisson equation can be solved, and the pressure is found by inverting the Υ operator. The last step in order to find velocity in the new time level is to perform a pressure correction which is completed by calculating equation (5)

$$\begin{aligned} (u)^{n+1} &= (u)^{\star} - (P_{\xi}\xi_x + P_{\eta}\eta_x)\Delta t \\ (v)^{n+1} &= (v)^{\star} - (P_{\xi}\xi_y + P_{\eta}\eta_y)\Delta t \end{aligned} \quad (40)$$

3.0 DISCUSSION OF NUMERICAL RESULTS

The developed computer code is investigated using standard incompressible flow problems: driven cavity flow, Taylor-Green (TG) vortex problem, double shear layer, backward-facing step, skewed cavity problem.

3.1 Driven Cavity Flow

The driven cavity flow problem is a benchmark problem used to validate the incompressible flow solver. It is extensively investigated because of certain flow features. Some interesting features of this problem are the following: boundary layer on the wall, flow separation from one wall and reattachment on the perpendicular wall, attachment and separation from the same wall, multiple separation and attachment, vortices, and bubbles. Detailed work was performed by Ghia, Ghia, and Shin in 1982. They employed second-order accurate central finite difference approximations for all the second-order derivatives in the continuity equation. Convective terms were represented by a first-order accurate upwind difference scheme including its second order accurate term as deferred correction. Two different uniform grid sizes of 129×129 and 257×257 were used for various Reynolds numbers. In the current computations, a grid size of 80×80 is utilized. The velocities u and v are taken to be zero on all boundaries except the top surface, where $u = 1$ and $v = 0$. As the initial condition, u and v are set to zero. Figure 1 illustrates the streamlines for the driven cavity flow at Re 100, 1000, and 3200. The primary vortex can be seen in the case when $Re = 100$. Two secondary vortices are also formed at the lower boundary. However, there is no upper secondary vortex formation since the Re is not sufficiently high. At $Re = 1000$, which is high, distinct secondary

upstream and downstream vortices are formed, with the primary vortex moving towards the geometric center of the cavity. As the flow velocity is increased, an upper secondary vortex is also formed in the case of $Re = 3200$. Solution of present scheme using 6400 nodes compare well with the published solution with 16641 nodes. Figure 2 (a, b, and c) shows the comparison of velocity profiles at $Re 100, 1000,$ and 3200 ; obtained by the current procedure with the results of Ghia et al. (1982).

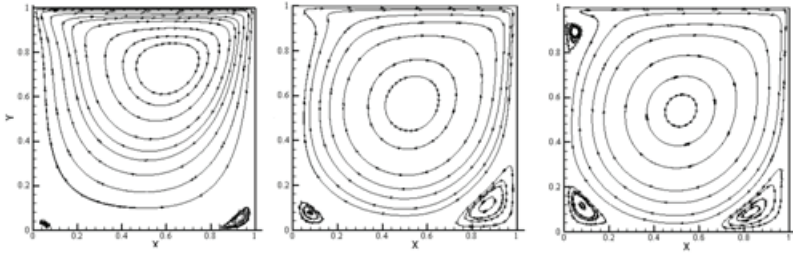


Figure 1. Streamlines of driven cavity at $Re = 100$ (left), 1000 (center) and 3200 (right) Grid resolution is 80×80 and time step is 0.001

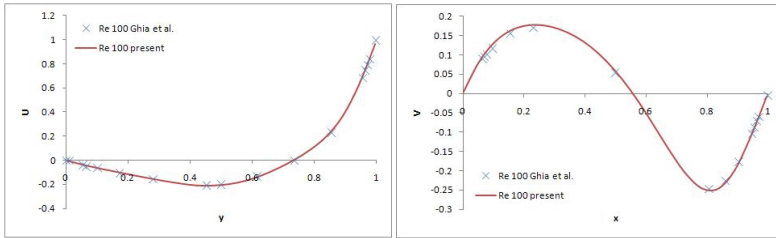


Figure 2(a). Comparison of velocity profiles at $Re = 100$ for the present and Ghia et al. (1982) study

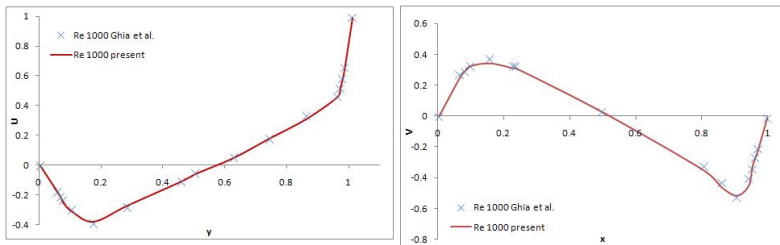


Figure 2(b). Comparison of velocity profiles at $Re = 1000$ for the present and Ghia et al. (1982) study

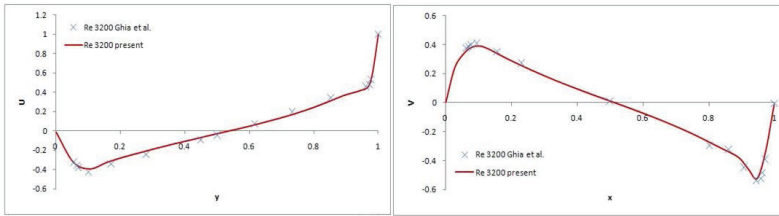


Figure 2(c). Comparison of velocity profiles at Re = 3200 for the present and Ghia et al. (1982) study

Table 1 shows the value of the vorticity and the location of the primary vortex center obtained by different researchers using different numerical methods. The difference in the results of the present study as compared to the highly accurate spectral solutions of Botella and Peyret (1998), extrapolated solutions of Schreiber and Keller (1983) and fourth order solutions of Erturk and Gokcol (2006), is very small. The current solutions are also comparing good with the other results of Wright and Gaskell (1995), Benjamin and Denny (1979), Nishida and Satofuka (1992), Erturk, et al. (2005) and Li et al. (1995) as shown in the table. The reason of reporting this table is to show that the results are obtained using very coarse grid and our proposition that WENO scheme resolves the flow with fewer grid points holds. The least amount of data points in the above table are 129×129 used by Li et al. (1995) whereas the grid points used in current study are 80×80 . All other numerical methods mentioned are using more grid points to achieve the said results. The similar location of the primary vortex center and close vorticity value indicates that the WENO scheme use is beneficial in getting the solution by using fewer grid points thus in the end saving the computational time of the computer and giving useful information about the flow characteristics.

Table 1. Vorticity value and location of the center of primary vortex by different studies

| Reference | Grid size | Accuracy | Vorticity | x | y |
|--------------------|-------------------|-----------------------|-----------|--------|--------|
| Botella & Peyret | N=160 | N=160 | 2.067753 | 0.5308 | 0.5652 |
| Schreiber & Keller | Extrapolated | 6 th order | 2.0677 | | |
| Erturk & Gokcol | 601 ² | 4 th order | 2.067760 | 0.5300 | 0.5650 |
| Wright & Gaskell | 1024 ² | 2 nd order | 2.06997 | 0.5308 | 0.5659 |
| Benjamin & Denny | Extrapolated | High order | 2.078 | | |
| Nishida & Satofuka | 129 ² | 8 th order | 2.068546 | 0.5313 | 0.5625 |
| Erturk et al. | 513 ² | 2 nd order | 2.064765 | 0.5313 | 0.5645 |
| Li et al. | 129 ² | 4 th order | 2.05876 | 0.5313 | 0.5625 |
| Current Study | 80 ² | 5 th order | 2.06893 | 0.5316 | 0.5642 |

3.2 Taylor Green Vortex Problem

The Taylor-Green vortex test problem has been widely used for verification of incompressible viscous flow solvers. The order of accuracy of the proposed solver is established by comparing the numerical results with the analytical values. A two-dimensional exact solution to the unsteady problem is provided by

$$\begin{aligned}
 u(x, y, t) &= -\cos(kx)\sin(ky)\exp(-2k^2t / \text{Re}) \\
 v(x, y, t) &= \sin(kx)\cos(ky)\exp(-2k^2t / \text{Re}) \\
 p(x, y, t) &= -\frac{1}{4}(\cos(kx) + \cos(ky))\exp(-4k^2t / \text{Re})
 \end{aligned}
 \tag{41}$$

The numerical domain of the numerical solutions is a square of side 2π with periodic boundary conditions in both x and y -directions. Uniform grid points of 32^2 , 64^2 , 128^2 , 256^2 and 512^2 are used in this convergence rate study. The order of accuracy of the proposed scheme is established by numerical simulation of the Taylor-Green vortex test at $\text{Re} = 100$, for 100 steps with a fixed time step of 0.001. The maximum error and the convergence rates are shown in (Table 2). It can be seen clearly that convergence rate of fifth order for the velocity variables is obtained as the grid is refined.

Table 2. Maximum error and convergence rates for TG vortex test

| Variable | 32^2 | Rate | 64^2 | Rate | 128^2 | Rate | 256^2 | Rate | 512^2 |
|----------|---------|------|--------|-------|---------|------|----------|-------|----------|
| u | 8.09e-4 | 3.7 | 6.2e-5 | 4.58 | 2.85e-6 | 4.99 | 0.897e-7 | 4.99 | .0281e-7 |
| v | 8.42e-4 | 3.52 | 7.3e-5 | 4.927 | 2.4e-6 | 5.01 | 0.745e-7 | 5.005 | .0232e-7 |

3.3 Double Shear Layer Test

The shear layer problem is an important numerical test in order to observe whether the numerical procedure is working properly when the solution of the problem is not smooth. This is a flow with a strong shear/discontinuous initial condition. A periodic boundary condition is applied everywhere on the boundaries and the initial condition of the jet is:

$$\begin{aligned}
 u_0(x, y) &= \begin{cases} \tanh(0.25 - y) / \rho, & y \leq 0.5 \\ \tanh(y - 0.75) / \rho, & y > 0.5 \end{cases} \\
 v_0(x, y) &= \delta \sin(2\pi x)
 \end{aligned}
 \tag{42}$$

Due to the initial condition, two shear layers are formed, since the velocity gradient is high at those two particular regions. In this case, the grid size is 256×256 . Figure 3 provides the vorticity contours at $t = 0.4, 0.8, 1.2,$ and 1.8 . These results are compared with the pioneering work

of Bell et al. (1989). The pattern obtained with the current approach is in good agreement with the result previously published for shear layer flow. No distortions or oscillations can be observed in the evolution of the flow over the specific time period, and no spurious vortices are seen.

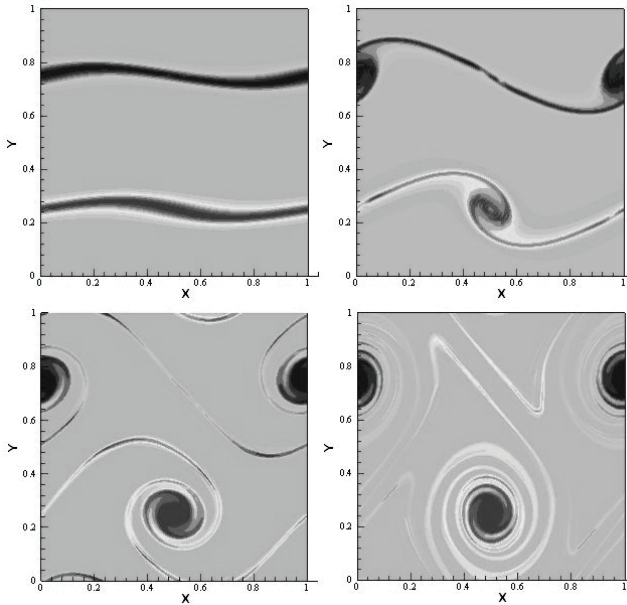


Figure 3. Vorticity contours for double shear layer flow at $t = 0.4$ (top left), 0.8 (top-right), 1.2 (bottom-left), and 1.8 (bottom-right)

In Figure 4, vorticity contours at $t = 1.8$ are shown for different grid sizes. It can be observed that even at the coarser grid the shape, location and number of vortices are maintained thus indicating the usefulness of WENO in getting the overall result by using fewer grid points. Figure 5 shows the plot of kinetic energy ($\int U \cdot U dx dy$) versus time for the double shear layer at two grid sizes of 128^2 and 256^2 . As the mesh becomes finer the kinetic energy stays unchanged for a longer period of time as compared to coarser grid. On comparing the current result of 256^2 grid size kinetic energy plot with the (Figure 4) in paper of Bell et al. (1989), it is seen that the kinetic energy is decreasing appreciably from the start of the solution whereas in the current solver it is constant up to $t \sim 1.1$. This clearly indicates that the new scheme has less dissipation than the original scheme of Bell. It is obvious to conclude that at meshes greater than 256^2 size the kinetic energy will be invariant for even greater time than 1.1.

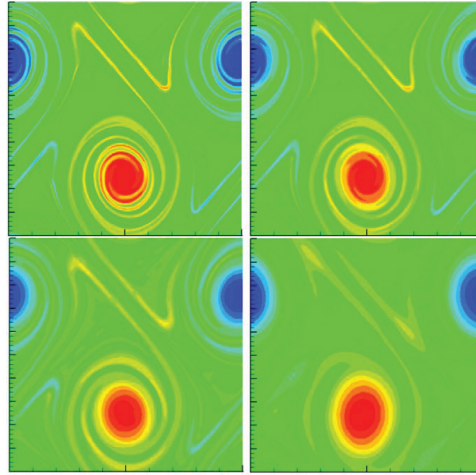


Figure 4. Vorticity contours for double shear layer flow at $t = 1.8$ for grid sizes of 256^2 (top left), 180^2 (top-right), 128^2 (bottom-left) and 64^2 (bottom-right)

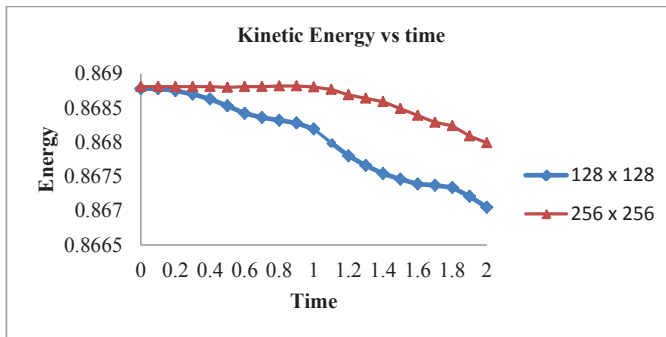


Figure 5. Kinetic energy versus time for double shear layer

3.4 Backward-Facing Step

Another commonly utilized benchmark problem is the flow over a backward-facing step. The dimensions of the step height and the channel length upstream and downstream are taken to be as reported in the experimental study of Armaly, Durst, Pereira and Schoung (1983) and the numerical study of Choi and Barakat (2005). The dimensions are sufficiently large so that the flow is fully developed when it reaches the step. The length of the channel downstream is such that the recirculation zone produced behind the step is independent of the rest of the channel length. For this problem, a multi-block meshing approach was utilized, and the Navier–Stokes solver was modified accordingly.

Geometric model of the back ward facing step used in this problem is given in Figure 6. Data points are obtained by digitizing the experimental data and comparing them to the numerical results, for a Newtonian fluid in Armaly et al. (1983). In order to do the meshing, the rectangle (700mm × 10.1mm) has been divided into four sub domains. The lower left sub rectangle has been made inactive in the calculations. The grid size of the left upper sub rectangle is 60 × 30 and the grid sizes of the right upper and right lower sub rectangles are 120 × 30. Figure 7 shows the comparison of velocity profiles obtained numerically with the experimental profiles at five positions downstream of the step. Two conclusions can be made by considering the comparison figures. First, the shape of the velocity profile obtained by the computer code is similar to the experimental profiles obtained by Armaly et al. (1983). The profile is parabolic right at the step, which indicates the fully developed flow. In the region where there is a circulation zone, the shape of velocity profile changes, but it becomes parabolic again as the flow moves downstream of the step. Second, the values of numerical simulation compare well with the experimental values. Figure 8 illustrates the comparison between the L/S (non-dimensional length of the recirculation zone) at different Reynolds numbers. Where L is the length of the channel after the step and S is the step height. The numerical values again compare well to the experimental values. Figure 9 provides the streamlines over the backward-facing step for Re = 50, 100, 200 and 400. It is clear that as the Re increases, the recirculation length also increases. The flow pattern is consistent with the results published by Choi and Barakat (2005) in their numerical study. It is worth mentioning that their computational domain consisted of 14,600 rectangular elements for the numerical simulations, whereas the current study is using only 9000 nodes to obtain the same results. The reason for this is that the WENO scheme has the inherent property of resolving flow even if a coarser grid size is used. Moreover, Choi et al. investigation uses the CFD software Fluent, which usually uses a third order solver for the spatial derivatives of N-S equations and second order solver for time discretization, where the current effort is making use of fifth and sixth order schemes to solve spatial derivatives (convective/diffusion) and a third order scheme for temporal discretization. The higher order schemes result in more accuracy due to less truncation error.



Figure 6. Geometric model of back ward facing step

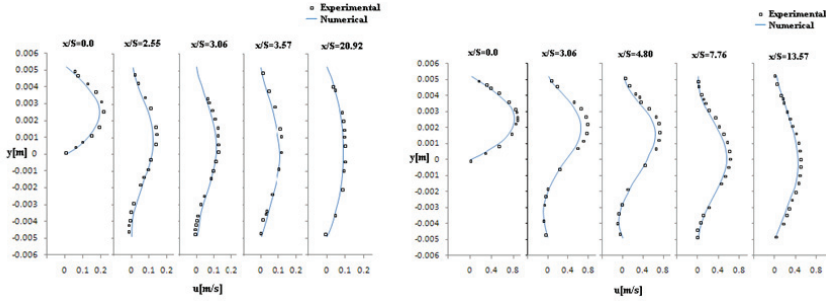


Figure 7. Axial velocity comparison for Newtonian steady flow at $Re=100$ (right) and $Re = 389$ (left)

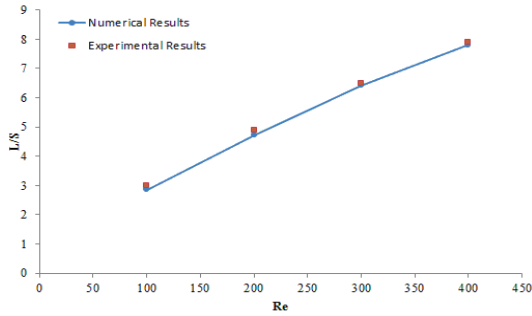


Figure 8. Non-dimensionalized length of recirculation region at different Re numbers

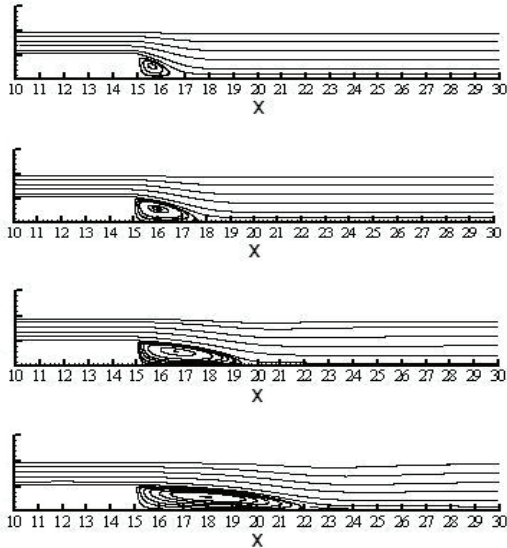


Figure 9. Streamlines of Newtonian flow at $Re = 50, 100, 200,$ and 400

3.5 Skewed Cavity

Up to this point all the examples analyzed are of rectangular geometry. As the problems in real life mostly comprise of non-rectangular geometries so to test the developed solver for such kinds of problems is very essential. Benchmark problems with non-rectangular grids for numerical schemes to compare solution to each other are not many. Demirdzic et al. (1992) presented the results for the skewed driven cavity for Re 100 and 1000 for the skewed angles of 45 and 30 degrees. Their results serve as a bench-mark solution for the non-rectangular grid test. The solution was obtained by using the multigrid finite volume method with grids up to 320×320 control volumes. This problem is simple to implement, and one can easily verify whether the code is functioning properly or not by comparing the results with the skewed cavity results of Demirdzic et al.. In the current study, a grid size of 128×128 (16,384 cells) is used, and the numerical results are in close agreement to the results of Demirdzic et al. (1992) that were obtained at 102,400 cells. Schematic of skewed driven cavity is drawn in (Figure 10). Figure 11 shows the u -velocity along the vertical line and v -velocity along the horizontal line passing through the geometric center of the skewed cavity for Re 100 and 1000 at the skewed angle of 45 degrees. Figure 12 illustrates the u -velocity along the vertical line and v -velocity along the horizontal line passing through the geometric center for Re 100 and 1000 at the skewed angle of 30 degrees. Other researchers that have performed the skewed driven cavity tests are Erturk and Dursun (2007), Oosterlee, Wessling et al. (1993) and Shyklyar and Arbel (2003) using the grid size of 513^2 , 256^2 and 320^2 respectively. This test clearly demonstrates that the proposed scheme is performing properly for the generalized coordinates in addition to the rectangular grid obtaining results at coarser grids when compared to the grid sizes of above mentioned researchers.

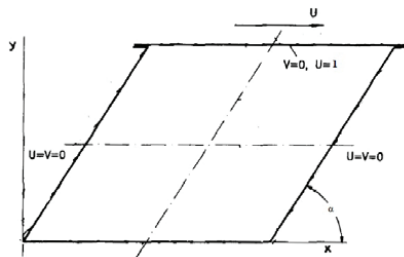


Figure 10. Geometric model of skewed driven cavity

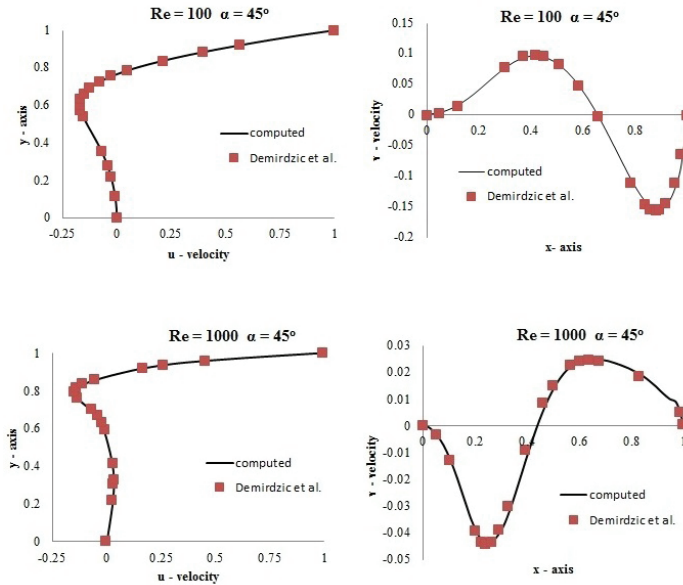


Figure 11. u and v -velocity profiles at $Re = 100$ and 1000 for skewed angle of 45 degrees

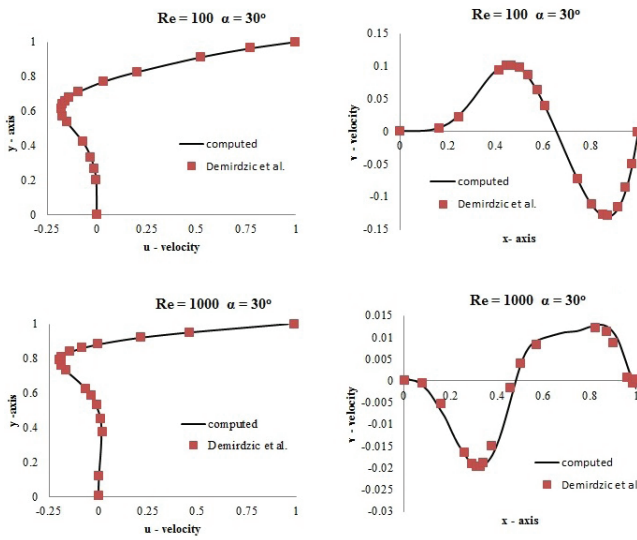


Figure 12. u and v -velocity profiles at $Re = 100$ and 1000 for skewed angle of 30 degrees

4.0 CONCLUSION

A WENO/compact scheme for solving the two-dimensional incompressible Navier-Stokes equations has been presented. The convective part of the N-S equations is solved using fifth order WENO spatial operators, and the diffusion terms are solved with a sixth-order compact central difference scheme. The third-order TVD Runge-Kutta explicit time-integrating scheme is adopted for the unsteady flow computations. Test cases, driven cavity flow, Taylor Green vortex test, double shear layer, and backward-facing step are performed to investigate the accuracy and efficiency of the scheme. Skewed driven cavity has been analyzed in order to study the functioning of proposed scheme in generalized coordinates. Bend tube is tested for codes functionality in three dimension with non-Newtonian and pulsatile flow. Results are compared with available established data in the literature and are in good agreement with the published data. It has been shown that due to the control adaptive dissipation property of WENO, the solver can capture the general flow features with coarser grid size. The code is thus grid efficient and fifth order accuracy is obtained for velocity variables. Another advantage of using this shock capturing scheme is that the developed code when extended to three dimensions can be used for the direct numerical simulation of the turbulence problems in future. Achieving the results by using fewer nodes will be very helpful in such kind of analysis in terms of computational efficiency.

REFERENCES

- Adams, N. and Shariff, K. (1996). A high-resolution hybrid compact-ENO scheme for shock-turbulence interaction problems. *Journal of Computational Physics*, 127, 27-51.
- Armaly, B. F., Durst, F., Pereira, J. C. F. and Schonung, B. (1983). Experimental and theoretical investigation of backward facing step flow. *Journal of Fluid Mechanics*, 127, 473-496.
- Arshed, G. M. and Hoffmann, K. A. (2009). Implementation of improved WENO scheme to higher dimensions in relation to shock-turbulence interaction. *Proceedings of 47th AIAA Aerospace Sciences Meeting*. AIAA-2009-1313, Orlando, Florida.
- Bell, J., Colella, P. and Glaz, H. (1989). A second order projection method for the incompressible Navier- Stokes equations. *Journal of Computational Physics*, 85, 257-283.

- Benjamin, A. S. and Denny, V. E. (1979). On the convergence of numerical solutions for 2-D flows in a cavity at large Re. *Journal of Computational Physics*, 33, 340-358.
- Botella, O. and Peyret, R. (1998). Benchmark spectral results on the lid-driven cavity flow. *Comput. Fluids*, 27, 421-433.
- Chen, Y. N., Yang, S. C. and Yang, J. Y. (1999). Implicit weighted essentially non-oscillatory schemes for the incompressible Navier-Stokes equation. *International Journal for Numerical Methods in Fluids*, 31, 747-765.
- Choi, H. W. and Barakat, A. I. (2005). Numerical study of the impact of non-Newtonian blood behavior on flow over a two dimensional backward facing step. *Biorheology*, 42, 493-509.
- Chorin, A. J. (1968). Numerical solution of the Navier-Stokes equations. *Mathematics of Computation*, 22, 745-762.
- Demirdzic, I., Lilek, Z. and Peric, M. (1992). Fluid flow and heat transfer test problems for non-orthogonal grids: Bench mark solutions. *International Journal for Numerical Methods in Fluids*, 15, 329-354.
- Drikakis, D. and Rider, W. (2005). High-resolution methods for incompressible and low-speed flows. Springer-Verlag, Berlin.
- Erturk, E., Corke, T. C. and Gokcol, C. (2005). Numerical solutions of 2-D steady incompressible driven cavity flow at high Reynolds numbers. *International Journal of Numerical Methods in Fluids*, 48, 747-774.
- Erturk, E. and Gokcol, C. (2006). Fourth order compact formulation of Navier-Stokes equations and driven cavity flow at high Reynolds Numbers. *International Journal of Numerical Methods in Fluids*, 50, 421-436.
- Erturk, E. and Dursun, B. (2007). Numerical solutions of 2-D steady incompressible flow in a driven skewed cavity. *Journal of Applied Mathematics and Mechanics*, 87, 377-392.
- Ghia, U., Ghia, K. N. and Shin, C. T. (1982). High-Re solutions for incompressible flow using the Navier-Stokes equations and a multigrid method. *Journal of Computational Physics*, 48, 387-411.
- Gijsen, F. J. H. (1998). *Modeling of wall shear stress in large arteries*. (PhD Dissertation). Eindhoven: Technische Universteit, Netherlands.
- Harlow, F. H. and Welsh, J. E. (1965). Numerical calculation of time dependent viscous incompressible fluid with free surface. *Phys. Fluids*, 8, 21-82.
- Harten, A., Engquist, B., Osher, S. and Chakravarthy, S. (1987). Uniformly high order essentially non-oscillatory schemes, III. *Journal of Computational Physics*, 71, 231-303.

- Hsieh, T. J., Wang, C. H. and Yang, J. W. (2008). Numerical experiments with several variant WENO schemes for Euler equations. *International Journal for Numerical Methods in Fluids*, 58, 1017-1039.
- Jiang, G. and Shu, C. W. (1996). Efficient implementation of weighted ENO schemes. *Journal of Computational Physics*, 126, 202-228.
- Kim, J. and Moin, P. (1984). Application of a fractional-step method to incompressible Navier-Stokes equations. *Journal of Computational Physics*, 59, 308-323.
- Ladeinde, F., O'Brien, E., Cai, X. and Liu, W. (1995). Advection by polytropic compressible turbulence. *Physics of Fluids*, 7, 2848-2857.
- Li, M., Tang, T. and Fornberg, B. (1995). A compact fourth order finite difference scheme for the steady incompressible Navier-Stokes equations. *International Journal of Numerical Methods in Fluids*, 20, 1137-1151.
- Liu, X. D., Osher, S. and Chan, T. (1994). Weighted essentially non-oscillatory schemes. *Journal of Computational Physics*, 115, 200-212.
- Moin, P. and Kim, J. (1980). On the numerical solution of time dependent viscous incompressible fluids flow involving solid boundaries. *Journal of Computational Physics*, 35, 381.
- Nishida, H. and Satofuka, N. (1992). Higher order solutions of square driven cavity flow using a variable order multi grid method. *International Journal of Numerical Methods in Fluids*, 34, 637-653.
- Oosterlee, C. W., Wessling, P., Segal, A., and Brakkee, E. (1993). Benchmark solutions for the incompressible Navier-Stokes equations in general co-ordinates on staggered grids. *International Journal of Numerical Methods in Fluids*, 17, 301-321.
- Orszag, S. A. and Israeli, M. (1974). Numerical simulation of viscous incompressible flow. *Annual Review of Fluid Mechanics*, 6, 281-318.
- Rogers, S. E. (1990). Numerical solution of incompressible Navier-Stokes equations. NASA TM 102199, Ames Research Center, Moffett Field, CA.
- Schreiber, R. and Keller, H. B. (1983). Driven cavity flow by efficient numerical techniques, *Journal of Computational Physics*, 49, 310-333.
- Shklyar, A. and Arbel, A. (2003). Numerical method for the calculation of incompressible flow in general curvilinear co-ordinates with double staggered grid. *International Journal of Numerical Methods in Fluids*, 45, 741-763.
- Shu, C. W. and Osher, S. (1988). Efficient implementation of essentially non-oscillatory shock capturing schemes. *Journal of Computational Physics*, 77, 439-471.

- Shu, C. W. and Osher, S. (1989). Efficient implementation of essentially non-oscillatory shock capturing schemes II. *Journal of Computational Physics*, 83, 32-78.
- Shu, C. W., Zang, T. A., Erlebacher, G., Whitaker, D. and Osher, S. (1992). High order ENO schemes applied to two- and three-dimensional compressible flow. *Applied Numerical Mathematics*, 9, 45-71.
- Shu, C. W. (1997). Essentially non-oscillatory and weighted essentially non-oscillatory schemes for hyperbolic conservation laws. NASA/CR-97-206253, Institute for Computer Applications in Science and Engineering, NASA Langley Research Center, Hampton, VA.
- Walsteijn, F. (1994). Robust numerical methods for 2D turbulence. *Journal of Computational Physics*, 114, 129-145.
- Wright, N. G. and Gaskell, P. H. (1995). An efficient multigrid approach to solving highly recirculating flows techniques. *Computer and Fluids*, 24, 63-79.

